

Multi-scale spectral characteristics of latent heat flux over flooded rice and winter wheat rotation system

Tao Zhang^a, Rangjian Qiu^{a,*}, Risheng Ding^b, Jingwei Wu^a, Brent Clothier^c

^a State Key Laboratory of Water Resources Engineering and Management, School of Water Resources and Hydropower Engineering, Wuhan University, Wuhan 430072, China

^b Center for Agricultural Water Research in China, China Agricultural University, Beijing 100083, China

^c The New Zealand Institute for Plant and Food Research Ltd, Mt Albert Road, Sandringham, Auckland 1025, New Zealand

ARTICLE INFO

Handling Editor - Dr R Thompson

Keywords:

Continuous wavelet transform
Latent heat flux
Orthogonal wavelet transform
Partial wavelet coherence
Rice-winter wheat field
Net radiation

ABSTRACT

The temporal variations of latent heat flux (λET) and its affecting factors vary from seconds to decades, and alter with crop species. Understanding the temporal coherence between λET and its influencing factors across different underlying surfaces is a crucial research topic with practical implications, and can enable better water management. To investigate this, we conducted a study in southern China measuring water and heat fluxes over flooded rice-winter wheat rotation fields from 2017 to 2021. Wavelet transform technology was employed to analyze the spectral properties of λET and its affecting factors. Results showed that the power spectra of λET exhibited different cascade laws for rice and winter wheat. The spectral variabilities of λET occurred at daily and seasonal time scales for both rice and winter wheat, and an additional weekly time-scale for rice. Furthermore, the cospectrum between λET and soil water content (SWC) for rice showed a significant temporal correlation at 2–4 days, indicating the period of water input. We found that the daily λET of both crops changed synchronously with daily net radiation (R_n), and preceded daily vapor pressure deficit (VPD) and air temperature (T_a) by 1.5–2.6 h. The phase angle between λET and T_a was significantly lower for rice (mean = 1.8 h) than winter wheat (mean = 2.3 h). Partial wavelet coherence revealed that R_n , followed by VPD, was the main meteorological factor affecting λET for the rotated flooded rice-winter wheat system at each time scale, especially at the daily time scale. Additionally, the effect of VPD on λET was lower for winter wheat than rice at scales below a month. These findings offered a useful insight into selecting models of λET for varying time scales and promoting better agricultural water management.

1. Introduction

Latent heat flux (λET) involves in water circulation and energy conversion, which are the most basic properties and functions of farmland ecosystems (Conway, 1987; Djaman et al., 2015; Yang et al., 2014). The majority of the water in the field is consumed by plant transpiration and soil evaporation (Rana and Katerji, 2000; Sutanto et al., 2012; Qiu et al., 2023). In addition, λET also has an important role in crop productivity and water use efficiency (Qiu et al., 2021). Furthermore, the interaction and feedback between microclimatic and plant physiological ecology can also be comprehensively represented by the dynamics of λET (Allen et al., 1998; Kişi, 2011). For instance, local and regional climate may change due to crop λET via affecting energy partitioning. On the other hand, the temporal variation of crop λET can be affected by

regional climatic changes (e.g. global warming) through affecting atmospheric evaporation capacity (Baldocchi et al., 2001). Hence, water management is critically dependent of understanding variations in λET .

Previous researches indicate that the controlling factors of λET change at varying time scales (Ding et al., 2013; Kang et al., 2003; Lei and Yang, 2010; Suyker and Verma, 2008). The main factor affecting λET is the eddy motion of atmospheric turbulence at the time scale less than hours (Katul et al., 2001), while is the eco-physiological, micro-meteorological, and soil moisture conditions from daily to monthly scales (Allen et al., 1998; Steduto and Hsiao, 1998), and is seasonal variation of climate and plant phenology from seasonal to annual scales (Baldocchi et al., 2001; Suyker and Verma, 2008). Furthermore, the temporal variations of λET for varying species are likely to be different. Therefore, it is of great importance to determine the temporal

* Corresponding author.

E-mail address: qiurangjian@whu.edu.cn (R. Qiu).

<https://doi.org/10.1016/j.agwat.2023.108471>

Received 28 March 2023; Received in revised form 1 August 2023; Accepted 2 August 2023

0378-3774/© 2023 The Authors. Published by Elsevier B.V. This is an open access article under the CC BY-NC license (<http://creativecommons.org/licenses/by-nc/4.0/>).

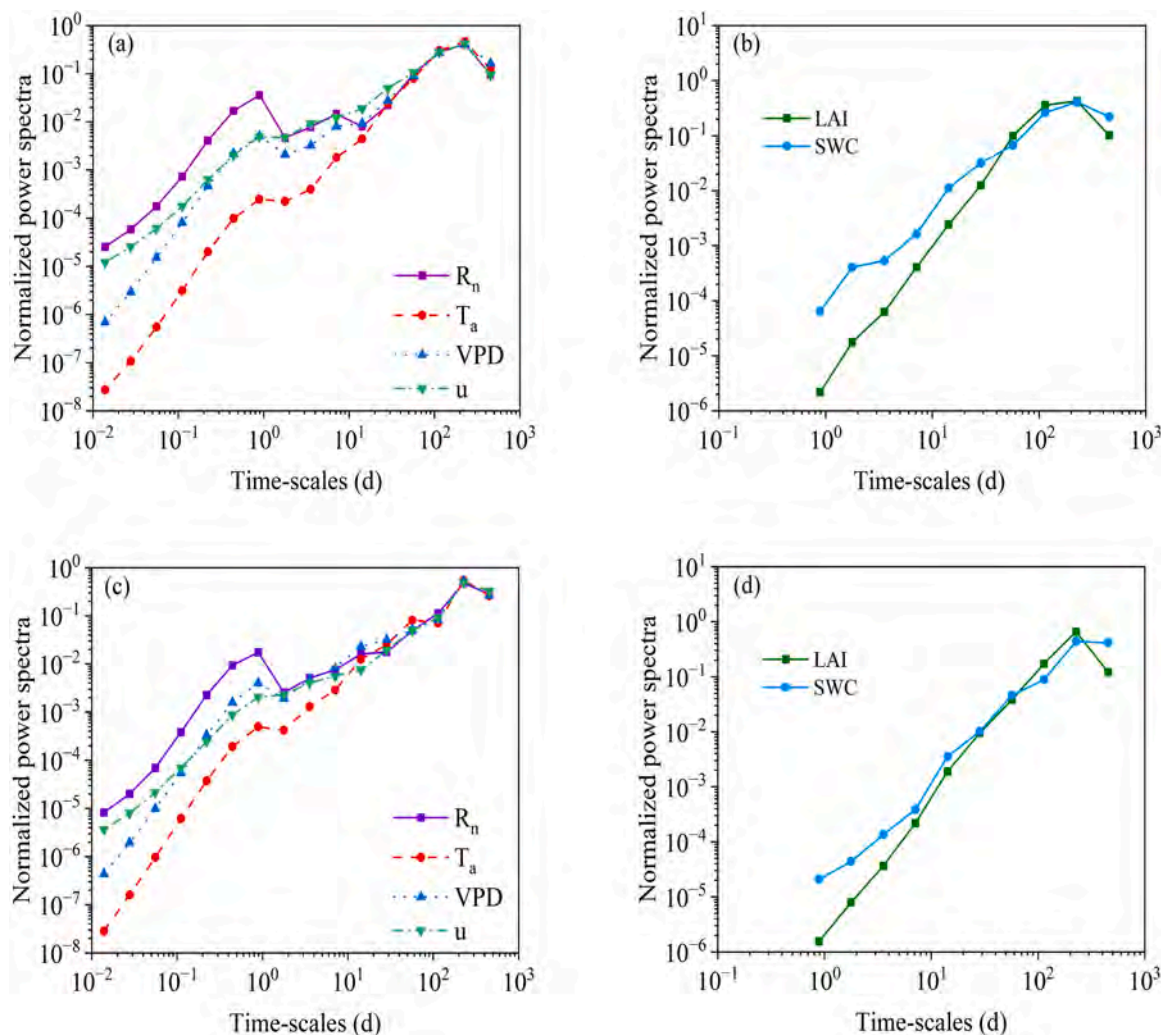


Fig. 1. Haar wavelet power spectra of net radiation (R_n), air temperature (T_a), vapor pressure deficit (VPD), wind speed (u), leaf area index (LAI), and mean soil volumetric water content in the 0–50 cm soil layer (SWC) for rice (a, b) and winter wheat (c, d).

characteristics of λET and its main influencing factors, which is beneficial to improve understanding of the mechanism for water and heat cycles and to determine the appropriate prediction models at varying time scales used for agricultural water management (Burba and Verma, 2005; Gong et al., 2021; Katul et al., 2001; Yan et al., 2022).

Wavelet transform can analyze non-stationary time series in the time-frequency domain (Gill et al., 2013; Kumar and Foufoula Georgiou, 1997), and this has been shown to be better than Fourier transform (Huang et al., 2010; Katul et al., 2001; Sifuzzaman et al., 2009). It has been widely used in many engineering applications and scientific research (Ding et al., 2013; Fawen et al., 2023; Mouatadid et al., 2019; Partal, 2009; Sen, 2009; Torrence and Compo, 1998; Vargas et al., 2010; Wang et al., 2022; Zhou et al., 2022). Wavelet transform has also been used to study the temporal pattern of λET over maize fields and its correlation with the main affecting factors on varying time-scales (Ding et al., 2013). In a subtropical coniferous plantation, Tang et al. (2021) used wavelet analysis to determine the spectral characteristics of net ecosystem productivity, evapotranspiration, as well as to identify the time lag between the fluxes and affecting factors. However, these studies mainly investigated the spectral information of water, heat, and carbon fluxes and their affecting factors from a single underlying surface (Ding et al., 2013; Tang et al., 2021). Agricultural systems can be complex and the varying growth conditions for different crops may change the spectral characteristics for water, heat, and carbon fluxes and their correlation with other factors (Hickman et al., 2010; Hu and Lei, 2021).

The rotated flooded rice-winter wheat system in southern China is the dominant cropping mode (10 % of the total arable land in China), where the flooded rice and winter wheat plants are grown during the period of May–October, and November–next May, respectively. This leads to a quite different magnitude and dynamics of λET for rice and wheat (Qiu et al., 2019). In addition, the effect of microclimate on hourly λET has also been reported to be different for rice and winter wheat (Qiu et al., 2019). Our former study has investigated the dynamics of λET and its correlation with influencing factors in the time domain (Qiu et al., 2019). However, the multi-scale spectral characteristics of λET and its main affecting factors over flooded rice and winter wheat rotation systems remain unclear.

Therefore, the objectives of this study are (1) to reveal the temporal patterns of λET and the main affecting factors for varying underlying surfaces; (2) to identify the temporal relationships between λET and its controlling factors at different time scales for two crops; (3) to study the degrees of correlation between λET and controlling factors for the different underlying surfaces.

2. Materials and methods

2.1. Experimental information

The water and heat fluxes measurements were carried out at five km away from the Agro-Meteorology Research Station in Nanjing, China

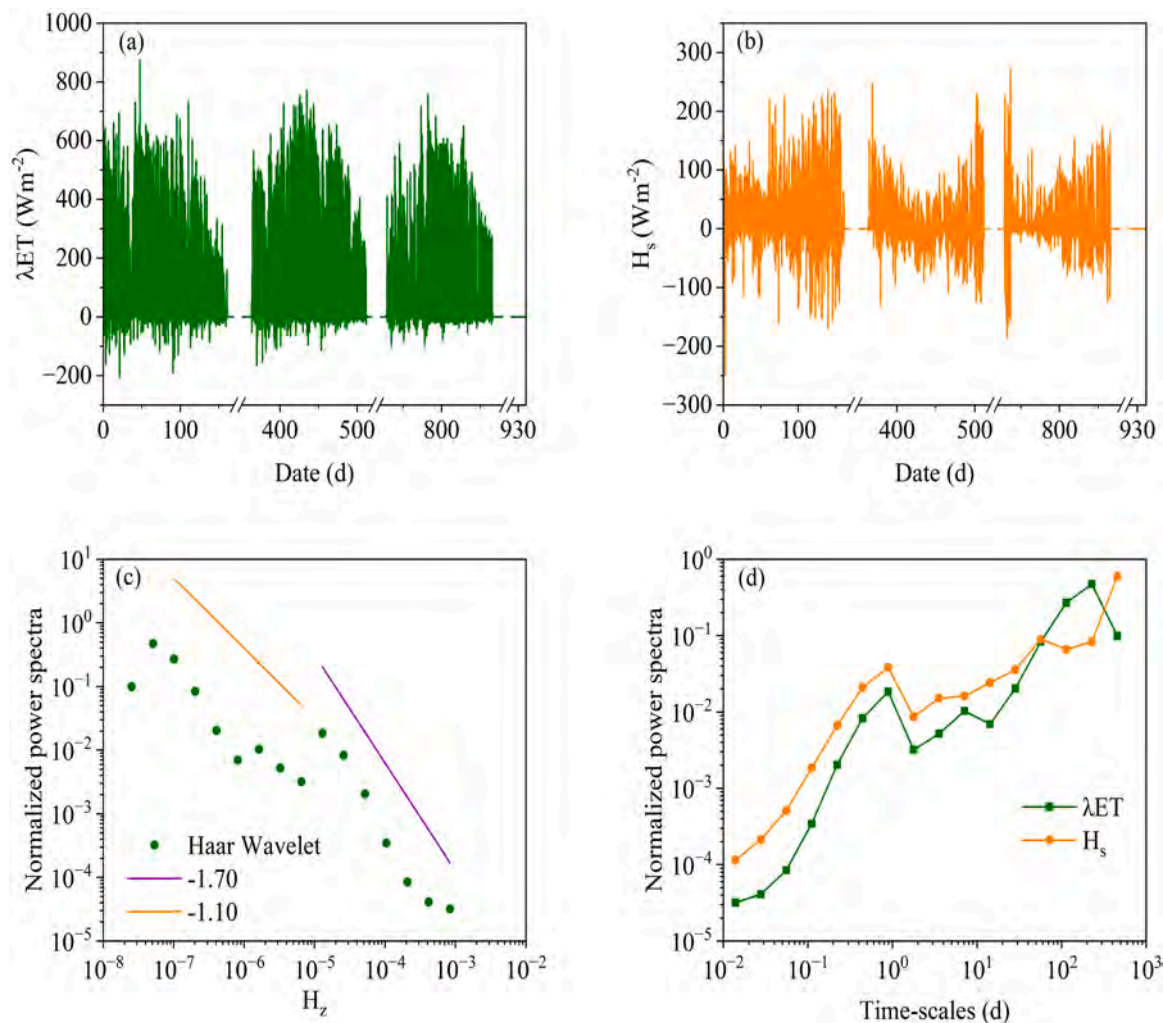


Fig. 2. Wavelet power spectra of 10 min water and heat fluxes for rice: (a) original time series of λET ; (b) original time series of sensible heat flux (H_s); (c) global power spectra of λET in the frequency domain by Haar wavelet transform and normalized by the variance of the relevant time series; (d) global power spectra of water and heat fluxes in the time domain.

(32°13'N, 118°41'E, altitude 14.4 m) from 2017 to 2021. The site has a subtropical monsoon climate. The annual air temperature is 15.4 °C, and precipitation is 1106 mm. The soil is classified as a silt loam. The mean bulk density of the soil in 0–50 cm is 1.53 g cm⁻³. The mean field water holding capacity and wilting point are 0.40 and 0.06 cm³ cm⁻³, respectively.

In this region, the dominant agricultural rotation is rotated flooded rice and winter wheat. In this experiment, the rice seeds (*Oryza sativa* L., cultivar Nanjing 5055) were direct sown in the field with sowing rate of 240 kg ha⁻¹ on June 1, 2018, May 30, 2019, and June 20, 2020, respectively, and harvested on November 8, 2018, October 30, 2019, and November 3, 2020, respectively, for 2018, 2019 and 2020 seasons. After the harvesting of rice, the winter wheat seeds (*Triticum aestivum* L., cultivar Ninmai 13) were direct sowing in the field with sowing rate of 300 kg ha⁻¹ on November 22, 2017, November 12, 2019, and November 7, 2020, respectively, and harvested on June 1, 2018, May 24, 2020, and May 27, 2021, respectively, for 2017–2018, 2019–2020, and 2020–2021 seasons. Wheat for the 2018–2019 season was not planted due to heavy and frequent precipitation during the last two months of 2018. The winter wheat plants were not suffered from water stress during the three growing seasons based on our former studies (Qiu et al., 2019, 2022).

The water and heat fluxes during the period 2017–2021 were measured using a Bowen-Ratio Energy Balance System (BREB) (Campbell Scientific, USA) installed in the north of the field (210 m × 100 m).

The detailed instruments installed are listed elsewhere (Qiu et al., 2022). Briefly, the system included one NR Lite2 net radiometer installed at 2.0 m height above the ground (above the crop canopy for at least 0.9 m) for monitoring net radiation, one CS320 digital thermopile pyranometer for measuring solar radiation, two 083E-1 temperature–humidity sensors mounted at 1.5 and 2.9 m heights for monitoring air temperature and relative humidity, two HFP01 heat flux plates for measuring soil heat fluxes at 0.05 m below the soil surface for rice and 0.08 m for wheat, four TT-T-24-SLE thermocouples for measuring soil temperature, one CS451 pressure transducer for measuring surface water level, five CS616 soil water content reflectometers installed in 0–50 cm soil layers for measuring soil water contents, one SI-111 infrared radiometer for measuring surface water temperature, one 034B wind monitor, and one TE525MM rain gauge. All data were recorded every 10 min by a CR1000 data logger. The detailed calculation procedure for water heat storage (F_w) and surface soil heat flux (G) is given in Qiu et al. (2019).

A canopy analysis system (LAI 2000, LI-COR Inc., USA) was employed to determine leaf area index (LAI) for the rice and winter wheat every 7–15 days. Then the Matlab software was applied to fit a temporal trend in the daily LAI.

2.2. BREB method and data management

The BREB method is determined based on energy balance method

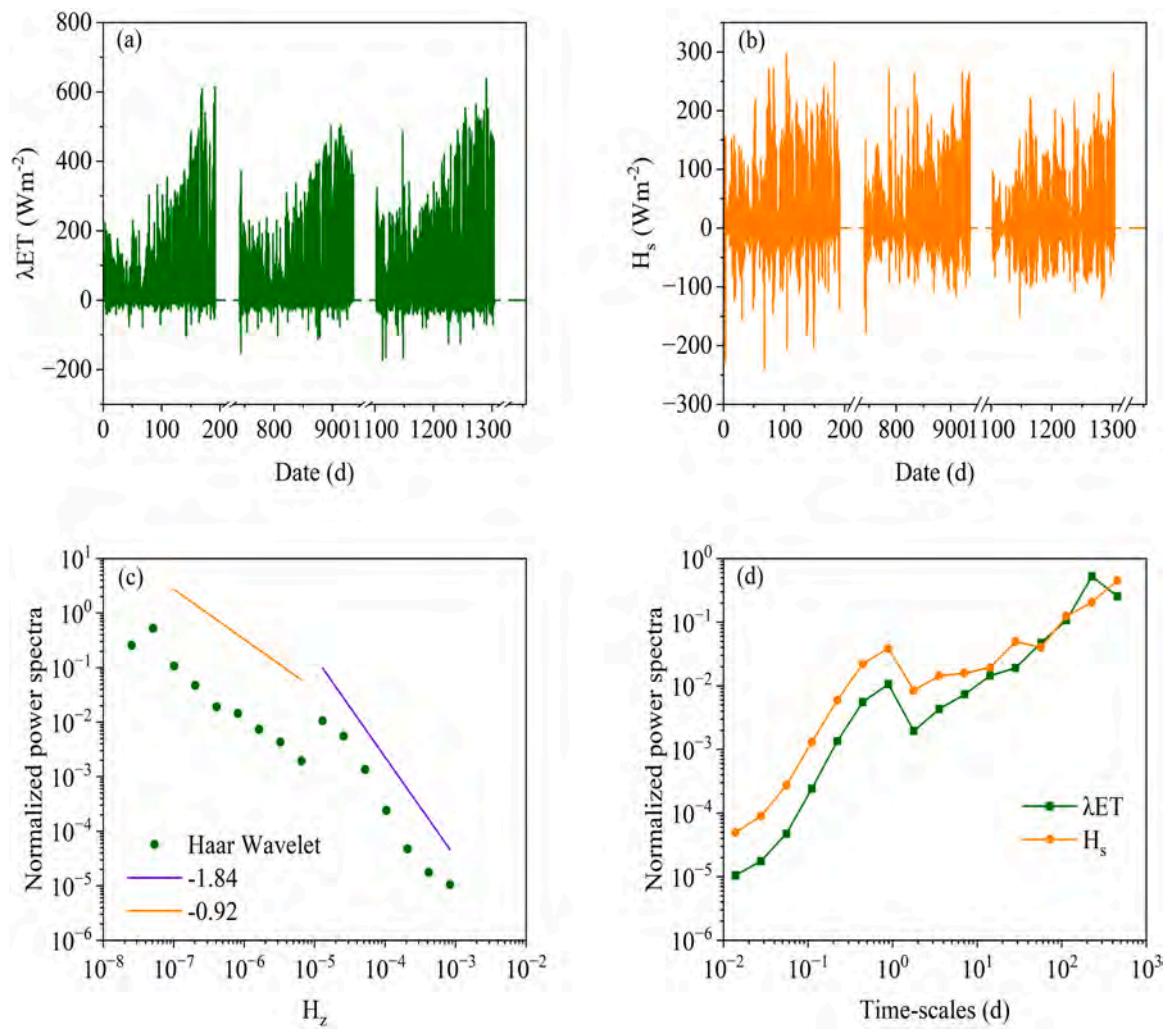


Fig. 3. Similar to Fig. 2, but for winter wheat.

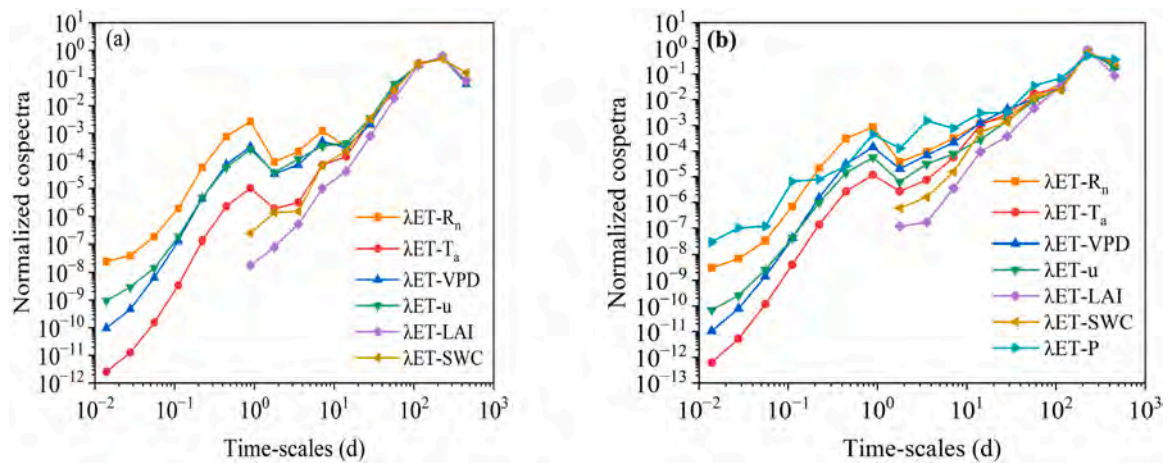


Fig. 4. Haar wavelet global cospectra between 10 min λET and net radiation (R_n), air temperature (T_a), vapor pressure deficit (VPD), wind speed (u), soil water content (SWC), and leaf area index (LAI), for rice (a) and winter wheat (b). The cospectra between λET and precipitation (P) for winter wheat is also shown in (b).

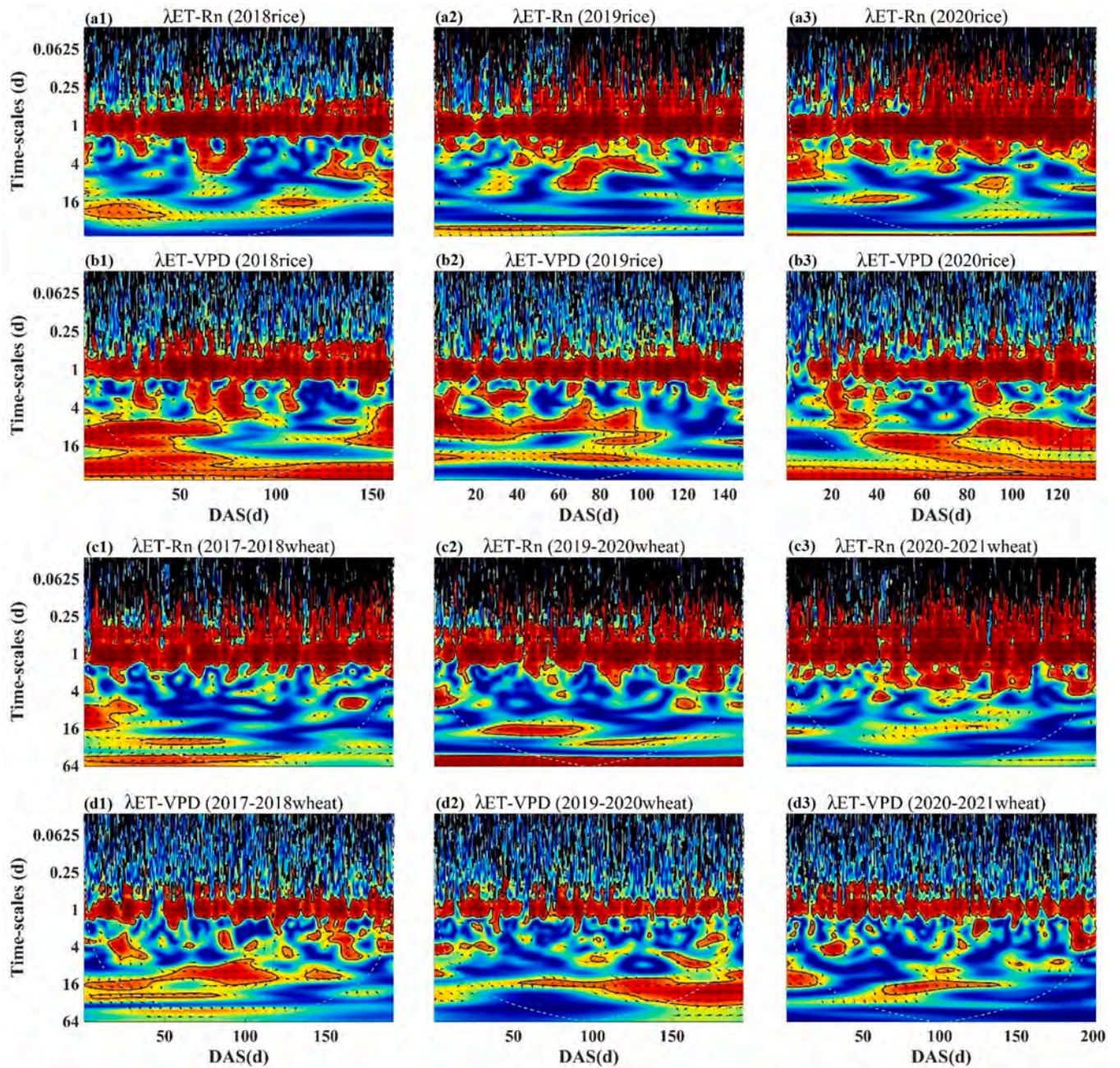


Fig. 5. Morlet wavelet coherence and phase spectra between λET and net radiation (R_n) and vapor pressure deficit (VPD) for rice and winter wheat. The DAS represents days after sowing.

and Bowen-ratio (β), as

$$R_n - G - F_w = \lambda ET + H_s \quad (1)$$

$$\beta = \frac{H_s}{\lambda ET} \quad (2)$$

where R_n is the net radiation ($W m^{-2}$); H_s is the sensible heat flux ($W m^{-2}$); F_w is 0 when there is no surface water. Combining Eqs. (1) and (2), λET and H_s can be calculated as

$$\lambda ET = \frac{R_n - G - F_w}{1 + \beta} \quad (3)$$

$$H_s = \frac{\beta}{1 + \beta} (R_n - G - F_w) \quad (4)$$

where $\beta \neq -1$. The β is determined based on the gradient of air temperature (T_a) and actual vapor pressure between the two heights

$$\beta = \gamma \frac{\Delta T}{\Delta e} \quad (5)$$

where γ is the psychrometric constant ($kPa \text{ } ^\circ C^{-1}$), ΔT and Δe are the difference of T_a ($^\circ C$) and actual vapor pressure between the two measured heights of 1.5 and 2.9 m in this study.

The data were continually measured during the growing period of rice and winter wheat. In addition, the information on quality-control of data and procedures of interpolation for the fluxes are shown elsewhere (Qiu et al., 2019). Briefly, all raw data were quality controlled based on the method proposed by Perez et al. (1999), depending on the physical inconsistency of the data and the resolution limitations of

Table 1

Mean phase angles of daily-scale latent heat fluxes (λET) and the meteorological factors for rice and winter wheat (h). \pm is the standard deviation. Different letters in the same column for mean values show significant differences at the $P < 0.05$ level.

Crop types	Year	$\lambda ET-R_n$	$\lambda ET-VPD$	$\lambda ET-T_a$	$\lambda ET-u$
Rice	2018	-0.7 \pm 0.4	1.7 \pm 0.7	1.5 \pm 0.9	0.3 \pm 1.5
	2019	-0.7 \pm 0.5	2.3 \pm 0.7	2.0 \pm 0.7	0.7 \pm 1.0
	2020	-0.6 \pm 0.8	2.0 \pm 1.0	1.7 \pm 0.8	0.5 \pm 1.1
	Average	-0.6 \pm 0.6a	2.0 \pm 0.8a	1.8 \pm 0.8b	0.5 \pm 1.2a
Winter wheat	2017–2018	-0.6 \pm 0.7	2.4 \pm 2.0	2.3 \pm 2.1	0.4 \pm 2.5
	2019–2020	-1.1 \pm 1.0	2.2 \pm 1.3	2.2 \pm 1.4	0.1 \pm 3.1
	2020–2021	-0.6 \pm 0.5	2.6 \pm 1.0	2.5 \pm 1.0	0.4 \pm 1.6
	Average	-0.8 \pm 0.8a	2.4 \pm 1.5a	2.3 \pm 1.5a	0.3 \pm 2.5a

temperature/humidity sensors. Overall, after quality control, more than 60 % of data for calculated λET and H_s are acceptable, and refused data are mainly appeared during night-time period. The refused λET fluxes were then interpolated by using a linear regression relationship between 10-min λET and available energy, which established every 4 days. The missing H_s values were interpolated by using energy residual method (i. e. $H_s = R_n - \lambda ET - G - F_w$). The data quality control and interpolation procedure has been developed by Matlab software, and the code has been freely shared in Github website: <https://github.com/shuilibite?tab=repositories>.

2.3. Research methodology

Power spectrum, cospectrum, coherence spectrum, phase-angle spectrum, and partial wavelet coherence (PWC) were used to analyze the time series. The variations of the variables (R_n , vapor pressure deficit (VPD), T_a , wind speed (u), soil water contents over 0–50 cm soil layers (SWC), and LAI) related to the specified frequencies can be represented by the power spectra (Kaimal et al., 1972). The covariant range of two different series can be expressed by the cospectrum (Baldocchi et al., 2001; Torrence and Compo, 1998). The phase-angle spectrum can show the consistency and sequence of changes for two different series (Grinsted et al., 2004), while PWC reflects the correlation degree of two different time series after the removal of an influence variable (Hu and Si, 2021). For instance, the PWC of $\lambda ET-R_n \sim VPD$ denotes partial wavelet coherence between λET and R_n after the removal of the influence of VPD . The meteorological factors investigated for PWC included R_n , VPD , and u in this study.

Since orthogonal wavelet transform (OWT) does not generate redundant data, its calculation speed is fast and the cost is low. These advantages make it suitable to analyze the global spectral features and some periodic features of time series in the frequency domain (Yoshida et al., 2010). However, the continuous wavelet transform (CWT) can analyze local information and correlation between two different series (Ding et al., 2013). The mother wavelet functions of the OWT and the CWT used in this study are the Haar function and the Morlet function. The OWT of time series $y(t)$ can be expressed as (Ding et al., 2013; Grinsted et al., 2004; Li et al., 2013; Torrence and Compo, 1998)

$$W_y(i, j) = \sum_{t=0}^{N-1} y(t) 2^{-\frac{i}{2}} \psi\left(2^{-i}t - j\right) \tag{6}$$

where $W_y(i, j)$ is the wavelet transform coefficient; $\Psi(t)$ is the mother wavelet function; N is the total number of time series, which is required to be an integer power of two; i is the number of an integer from 0 to $M-1$ ($M = \log_2 N$); j takes the value of an integer from 0 to 2^{M-i} .

The global power spectrum (P_y) is the mean squared difference of whole wavelet coefficients in the scale range, determined as (Ding et al., 2013)

$$P_y(i) = \frac{1}{2^{M-i}} \sum_{j=0}^{2^{M-i}-1} (W_y(i, j))^2 = \overline{(W_y(i, j))^2} \tag{7}$$

where $\overline{(\quad)}$ is the mean value. For two different time series $x(t)$ and $y(t)$, the cospectrum (Co_{xy}) is calculated as

$$Co_{xy}(i) = \overline{(W_x(i, j) \cdot W_y(i, j))} \tag{8}$$

where $W_x(i, j)$ and $W_y(i, j)$ are the wavelet transform coefficients of the two time series. In this study, the total number of time series for the 10 min values of λET is 64,369 and 84,816, respectively, for rice and winter wheat over three growing seasons. Since the amount of data in the time series of the OWT should be an integer power of two, 2^{17} (131,072) is the closest power of two for both crops, and the time series for non-growing period were interpolated by 0. According to the Nyquist frequency, the highest frequency is 50 % of the sampling. Hence, the number of coefficients of 10 min λET for both crops after the OWT is 2^{16} . The lowest and highest frequencies corresponding to OWT are 2.54×10^{-8} and 8.33×10^{-4} Hz which correspond to 455 d and 20 min for 10 min λET .

If $y(t)$ is square integrable, $y(t) \in L^2(R)$, then the CWT of $y(t)$ (W_y) can be obtained as follows (Li et al., 2013; Mallat, 1999)

$$W_y(m, n) = \frac{1}{\sqrt{m}} \int_0^{n-1} y(t) \psi^*\left(\frac{t-n}{m}\right) dt, m > 0 \tag{9}$$

where m is the scale factor reflecting the size of the period; n is the translation factor reflecting the shift in time; Ψ^* is the complex conjugate of the mother wavelet function (Sen, 2009); m and n varied depending on differences of wavelet functions. The cross spectrum (G_{xy}) is expressed as

$$G_{xy}(m, n) = W_x(m, n) W_y^*(m, n) \tag{10}$$

where W_y^* is the complex conjugate of W_y .

The expression of the coherence spectrum ($Co_{h_{xy}}$) is given by

$$Co_{h_{xy}}^2(m) = \frac{|\langle s^{-1} G_{xy}(m, n) \rangle|^2}{\langle s^{-1} |W_x(m, n)|^2 \rangle \langle s^{-1} |W_y(m, n)|^2 \rangle} \tag{11}$$

where $\langle \rangle$ is the smoothing of time and scale; s^{-1} can convert energy to power spectral density; the definition of coherence spectrum is similar to correlation, which refers to the local correlation of time series in the wavelet time-frequency space (Grinsted et al., 2004). The spectral angle spectrum (Φ_{xy}) represents complex argument of cross spectrum (G_{xy}) and its expression is

$$\Phi_{xy}(m) = \tan^{-1} \left(\frac{I\{\langle s^{-1} G_{xy}(m, n) \rangle\}}{R\{\langle s^{-1} G_{xy}(m, n) \rangle\}} \right) \tag{12}$$

where I is the imaginary part of the complex function; and R is its real part. The phase angle represents the before and after changing of the order of two time series in the time-frequency domain, its range is -180° to 180° .

The PWC analysis between the time series $x(t)$ and $y(t)$ without considering one variable $Z(t)$ at scale s and location τ , and $\rho_{y,x,Z}$ can be expressed as follows (Hu and Si, 2021)

$$\rho_{y,x \bullet Z}^2 = \frac{|\gamma_{y,x}(s, \tau) - \gamma_{y,Z}(s, \tau) \overline{\gamma_{x,Z}(s, \tau)}|}{(1 - R_{y,Z}^2(s, \tau))(1 - R_{x,Z}^2(s, \tau))} \tag{13}$$

where $\gamma_{y,x}(s, \tau)$ is the complex wavelet coherence between y and x ; the symbol \bullet is the notation for excluding variables; $R_{y,x,Z}^2(s, \tau)$, $R_{y,Z}^2(s, \tau)$, and $R_{x,Z}^2(s, \tau)$ can be calculated from (Hu and Si, 2016)

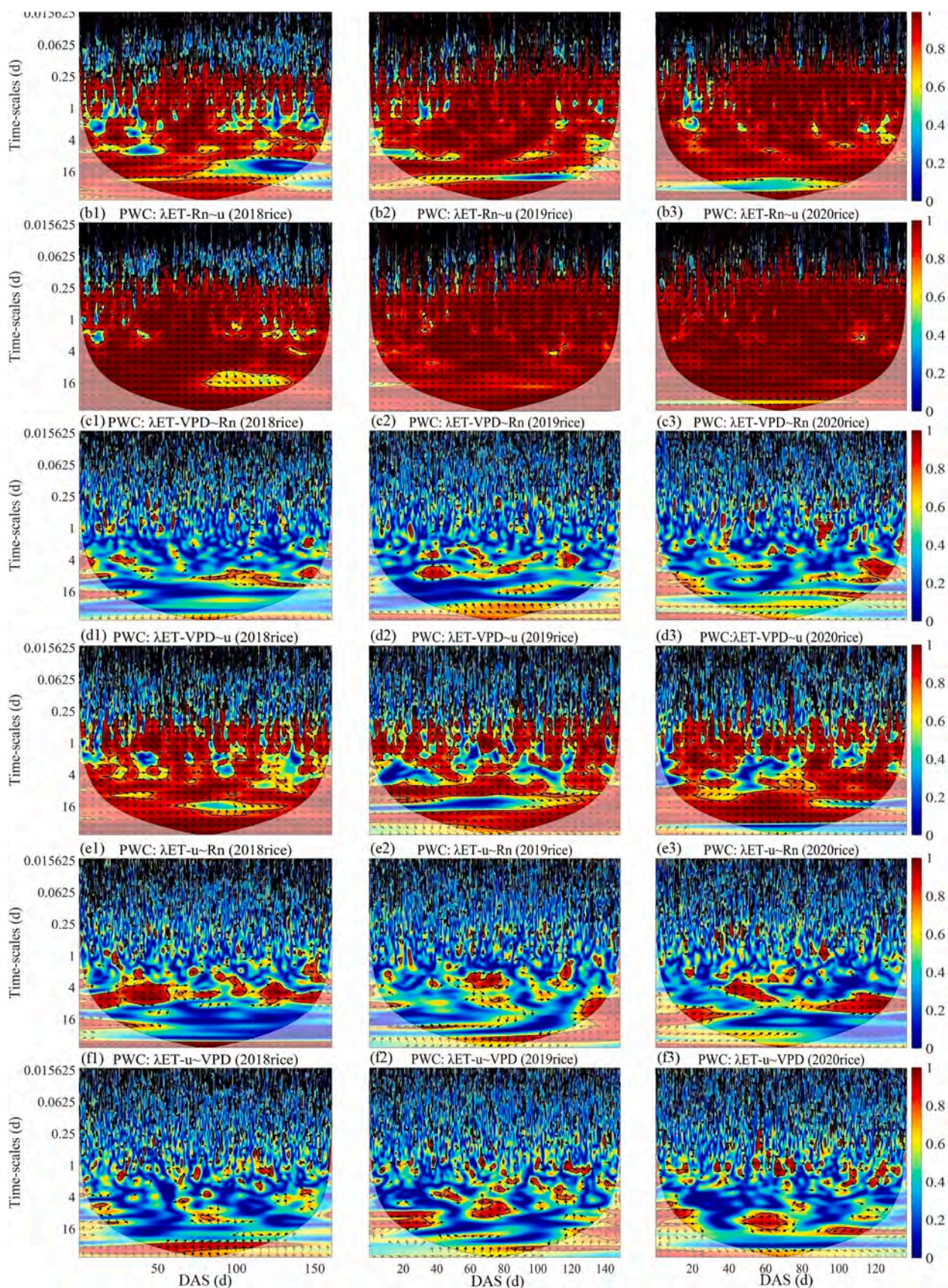


Fig. 6. Partial wavelet coherence of rice latent heat flux (λET) in combination with net radiation (R_n), vapor pressure deficit (VPD), and wind speed (u). The DAS represents days after sowing.

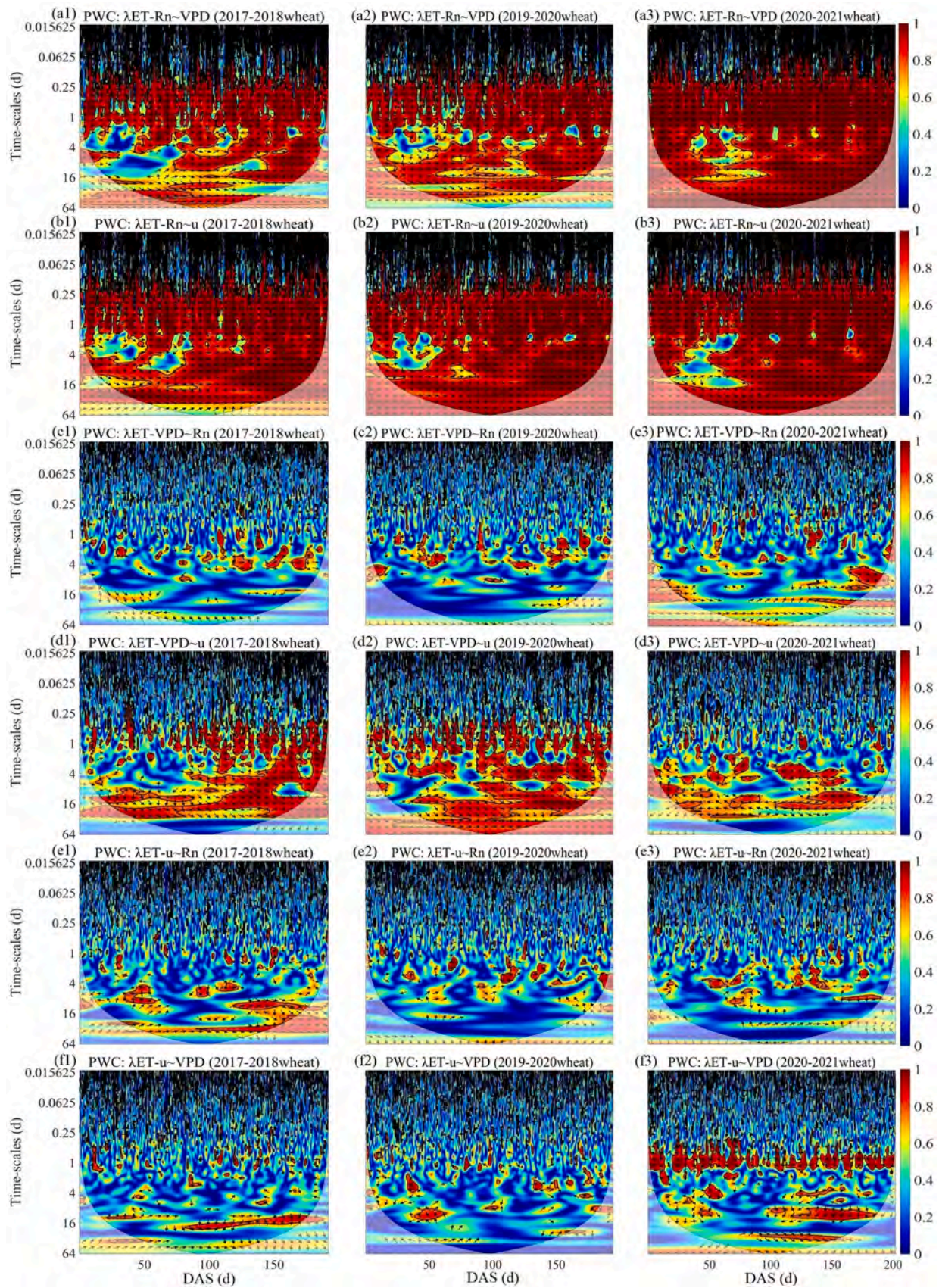


Fig. 7. Similar to Fig. 6, but for winter wheat.

$$R_{y,x,z}^2(s, \tau) = \frac{\overleftarrow{w}^{y,z}(s, \tau) \overleftarrow{w}^{z,z}(s, \tau)^{-1} \overleftarrow{w}^{x,z}(s, \tau)}{\overleftarrow{w}^{y,x}(s, \tau)} \quad (14)$$

$$R_{y,z}^2(s, \tau) = \frac{\overleftarrow{w}^{y,z}(s, \tau) \overleftarrow{w}^{z,z}(s, \tau)^{-1} \overleftarrow{w}^{y,z}(s, \tau)}{\overleftarrow{w}^{y,y}(s, \tau)} \quad (15)$$

$$R_{x,z}^2(s, \tau) = \frac{\overleftarrow{w}^{x,z}(s, \tau) \overleftarrow{w}^{z,z}(s, \tau)^{-1} \overleftarrow{w}^{x,z}(s, \tau)}{\overleftarrow{w}^{x,x}(s, \tau)} \quad (16)$$

where $R_{y,x,z}^2(s, \tau)$ is a matrix with complex values; $R_{y,z}^2(s, \tau)$ and $R_{x,z}^2(s, \tau)$ are matrices with real numbers; $\overleftarrow{w}^{ij}(s, \tau)$ indicates the smoothing operator; $(\)^{-1}$ is the inverse of the matrix; $\overline{(\)}$ indicates the complex conjugate operator; $\overleftarrow{w}^{ij}(s, \tau)$ is the smoothed auto-wavelet power spectrum (if $i = j$) or cross-wavelet power spectrum (if $i \neq j$) at scale s and location τ . According to the definition of complex coherence between two variables in the time-frequency space, the complex wavelet spectrum in the frequency domain can be deduced (Hu and Si, 2021). Detailed operational steps can be found elsewhere (Hu and Si, 2021).

We employed the Monte Carlo method to measure the significant differences of the wavelet transform coherence at the 95 % confidence level (Grinsted et al., 2004). Wavelet transform and wavelet analyses were performed in MATLAB software using the WAVELAB 850 packages (<https://statweb.stanford.edu/~wavelab/>).

3. Results and discussion

3.1. Wavelet power spectra for affecting factors of λET

The Haar-wavelet global power spectrum can reflect the fluctuation status of different factors, which is useful for analyzing the dynamics of λET and other factors. Figs. 1a and 1c showed that the power spectra of R_n , T_a , VPD , and u had similar characteristics for both rice and wheat. They all exhibited significant spectral peaks at the daily scale, reflecting the diurnal variation of meteorological factors relating to day-night variation (Ding et al., 2013). The power spectrum of R_n on daily time-scale was the greatest among these meteorological elements, indicating R_n had the largest fluctuation on daily time scale (Baldocchi et al., 2001; Ding et al., 2013; Steduto and Hsiao, 1998). However, the magnitudes of the spectral peaks of these four factors differed at the daily level. The power spectrum magnitude for R_n was one order greater than that for VPD and u , and was two orders greater than that for T_a (i.e. ranking of $R_n > VPD > u > T_a$), which is consistent with that found by Ding et al. (2013). However, for winter wheat the ranked order of magnitude for the power spectra was $R_n > VPD > T_a > u$. In addition, the spectral peaks were also observed at the 228d time-scale with similar magnitudes for the four factors for both rice and winter wheat, showing that meteorological factors had seasonal variations (Ding et al., 2013). Different from the wavelet power spectra for winter wheat, the power spectrum of R_n for the growing period of rice also showed a weekly spectral peak, which indicates that R_n also fluctuates at the weekly scale (Tyagi et al., 2000). However, the R_n for the growth period of winter wheat did not have this feature.

Compared to the power spectra of the meteorological factors, the power spectra for LAI showed a spectral cascade from daily to seasonal time-scale (Figs. 1b, 1d), showing the role of the growth period of LAI and crop phenology (Ding et al., 2013). The power spectrum of LAI at the 228 d scale was the greatest, and more than five orders of magnitude greater than the daily scale for both rice and winter wheat (Figs. 1b, 1d), although there was a plateau between 114 d and 228 d for rice. Power spectra for SWC showed a spectral cascade for both rice and wheat, and peaked at 228 d.

3.2. Wavelet power spectra of λET and H_s , and cospectra between λET and affecting factors

Since the meteorological conditions change over years and the growth periods, the time series of λET and H_s showed differences and non-stationary characteristics for the three growing seasons (Figs. 2a, 2b; Figs. 3a, 3b). The peak values of λET mainly appeared in the middle stages for rice and the late stages for winter wheat (Figs. 2a, 3a). However, there was no fixed period for the peak for H_s , and it also varied between years (Fig. 2b, Fig. 3b). Note that there are some negative values of λET during the night (indicating condensation) for both rice and winter wheat, which are generally appeared when vapor pressure gradients are greater than 0 (i.e. vapor pressure in the upper measurement level is greater than the lower measurement level) (Perez et al., 1999).

The global power spectra of λET had different power cascades before and after 1.30×10^{-5} Hz for both rice and winter wheat (Figs. 2c, 3c). The power laws were -1.10 and -0.92 (Figs. 2c, 3c), respectively, for rice and winter wheat between 1.02×10^{-7} and 1.30×10^{-5} Hz, and -1.70 and -1.84 , respectively, from 1.30×10^{-5} to 8.33×10^{-4} Hz (Figs. 2c, 3c). These results also indicated that the cascade power law of rice is different from that of winter wheat in the range of 1.02×10^{-7} – 8.33×10^{-4} Hz (Figs. 2c, 3c). The time domain of power spectra of λET and H_s for rice and winter wheat ranged from 20 min to 455 d (Figs. 2d, 3d). The fluctuation of λET on the 228d time scale is two orders of magnitude higher than the daily fluctuation of spectral energy (Figs. 2d, 3d) and the magnitude of the change is different between seasons. Similar results were also reported in former study (Ding et al., 2013). Hence, it is necessary to determine λET in long-time series, as this is crucial for promoting regional water management (Howell et al., 1998; Zhang et al., 2011). In addition, the global power spectra of λET also showed peaks at daily and weekly scales for rice, but only at the daily scale for winter wheat (Figs. 2d, 3d). The spectral peak of λET appeared on the daily time-scale, which is consistent with the daily fluctuation of λET reported in previous study (Allen et al., 1998; Ding et al., 2013; Howell et al., 1998). Furthermore, the daily and seasonal spectral peaks of λET indicate that λET has diurnal and seasonal variations. Hence, the determination of the growth period data in multiple years is necessary, which is conducive to the improvement of water resource utilization efficiency (Howell et al., 1998; Zhang et al., 2011).

Since the spectral characteristics of the global power spectra of λET corresponded to those of R_n and VPD (Figs. 1a, c; 2d, 3d), and H_s is not significantly correlated with these, we only analyzed the relationships between λET and the affecting factors. The cospectra between λET and R_n was highest on the daily scale showed that daily λET may change with daily R_n synchronously (Ding et al., 2013). In addition, the cospectra between daily λET and precipitation for winter wheat was also high (Fig. 4b), indicating precipitation has great effect on daily λET of winter wheat. For different scales, the greatest cospectra between λET and affecting factors for rice and winter wheat were both around 228 d, followed by the daily scale (Fig. 4). In addition, the weekly spectral peaks between λET and both R_n and VPD were also observed for rice, showing that the dynamic relationship between λET and R_n and VPD will change on a weekly time scale (Tyagi et al., 2000). Furthermore, the markedly increased cospectra between λET and T_a from the 15 d to 228 d scale indicates an enhanced correlation over the medium-term for rice and winter wheat. A similar magnitude of cospectra between λET and all factors at the 228 d scale shows that the long-term variability of λET was generally affected by all factors (Ding et al., 2013). However, at the daily scale, the cospectra between λET and SWC and LAI were lower than those of λET and the meteorological factors. The cospectra of λET and SWC appeared on the 2–4 d time-scale platform for rice, which may reflect the interval of the irrigation, plus any precipitation. On the contrary, the absence of a platform in the co-spectra of λET and SWC for wheat related to the irregular precipitation during the growth period of wheat since there is no irrigation event for winter wheat in Southern

China (Qiu et al., 2019). This is different from previous study, which reported that the cospectra between λET over maize field and SWC showed a flat region between the 5–10d time scale in northern China (Ding et al., 2013).

3.3. Coherence spectra and phase-angle spectra for relationships between λET and affecting factors

Since the correlations between λET and both T_a and u on the daily scale are not very high, the coherence spectra are not shown. During the three growth seasons for rice and winter-wheat, close relationships between λET and R_n were observed at or less than daily time scale based on the coherence spectra analysis (Fig. 5), indicating that R_n is the main driving variable of λET at these time scales (Ding et al., 2013; Lei and Yang, 2010; Qiu et al., 2019; Suyker and Verma, 2008). This provides theoretical basis for the application of radiation-based λET estimation models, such as the Priestley-Taylor method. Previous study showed that the modified Priestley-Taylor model can better estimate the short-term and daily λET (Qiu et al., 2019, 2021, 2023). On the daily time scale, λET also showed a good correlation with VPD. The phase-angle spectra at the daily scale showed that λET lagged behind R_n by 0.6 h for rice, and 0.8 h for winter wheat (Table 1). In contrast, λET preceded VPD by ~ 2 h for rice and 2.4 h for winter wheat (Table 1). The phase-angle relationships between λET and T_a were similar to that between λET and VPD (Table 1). Although the phase relationships between λET and meteorological factors are similar with those reported (Ding et al., 2013; Tang et al., 2021), the preceded and lagged times are different. In addition, there were significant ($P < 0.05$) differences in the phase angle between λET and T_a for rice (mean = 1.8 h) and winter wheat (mean = 2.3 h) (Table 1). Furthermore, the relationship between λET and u was weak when compared to that between λET and other meteorological factors (Ding et al., 2013; Qiu et al., 2019).

3.4. Partial wavelet coherence for λET and main factors

The PWC can be used to analyze the local relationship of two different series after the removal of an influencing variable at a specific scale (Hu and Si, 2021). According to the result of this PWC (Figs. 6, 7), the correlations between λET and R_n after removing the influence of VPD and u were still higher at or less than the daily time-scale. But λET had little correlation with VPD or u after removing the effect of R_n , indicating that R_n is the major influencing variable of λET at or less than the daily scale (Ding et al., 2013; Qiu et al., 2019; Tang et al., 2021). This is because solar radiation affects T_a and humidity, and these control stomata opening and affect transpiration (Qiu et al., 2019). In addition, the correlation between λET and R_n without considering the VPD of rice was more affected than that of wheat at or less than the daily scale (Figs. 6, 7). This shows that the correlation between λET and R_n was less affected by VPD for winter wheat than for rice at this time-scale (Qiu et al., 2019).

From the daily to monthly time-scale, the correlation between λET and R_n after removal of VPD for rice and winter wheat was discontinuous. This indicates that VPD has an indirect impact on the correlation between λET and R_n at this scale (Tang et al., 2021). However, Qiu et al. (2019) showed that the main indirect impact of R_n on λET is through the pathway of VPD on λET at 10 min time scale using path analysis.

The correlation between λET and u after removal of R_n or VPD was insignificant and discontinuous at all time scales. In addition, the correlation between λET and u after removal of VPD was weaker than that between λET and VPD after the removal of u . This shows that u has the weakest impact on the λET for both rice and winter wheat.

4. Conclusions

The λET is different in response to varying affecting factors for rice and winter wheat at different time scales, and the processes of λET for

rotated rice-wheat system is complicated. In this study, we employed the wavelet transform method to analyze the spectral characteristics and driving relationships of λET and determine the main affecting factors for flooded rice-winter wheat rotation system. We found that the power spectra of λET in the frequency domain had cascade power law and the power law changed at 1.30×10^{-5} Hz (corresponding to 1d). The cascade power laws were -1.1 for rice and -0.92 for wheat from 1.02×10^{-7} Hz to 1.30×10^{-5} Hz, and they were about -1.70 for rice and -1.84 for wheat from 1.30×10^{-5} to 8.33×10^{-4} Hz. In addition, the global power spectra of λET in the time domain peaked at the diurnal and seasonal time-scales for both rice and winter wheat, and for additional weekly time-scale for just rice. This indicates the varying changes of λET under different underlying surfaces. Based on the diversity of time-scale information for λET , the above characteristics of λET should be considered in the empirical and physics models to accurately predict the dynamic variation of λET .

The cospectra between λET and R_n for both rice and winter wheat were greatest on the daily scale indicating that λET changed synchronously with daily R_n . A similar magnitude of co-spectra between λET and all factors at 228d showed that the seasonal λET was dominated by all affecting factors. In addition, the weekly covariant changes between λET and both R_n and VPD were also observed for rice. Phase-angle spectral analysis showed that λET lagged R_n , while it preceded VPD and T_a at the daily scale for both rice and winter wheat. In addition, the phase-angle between λET and T_a was significantly greater for winter wheat than rice. Partial wavelet-coherence analysis indicated that R_n was the main meteorological factor for λET , followed by VPD for all scales, especially for daily scale. In addition, the λET of rice was more affected by VPD than winter wheat, and u was the weakest among all meteorological factors. These support the selection of appropriate methods to predict λET for different crop species and crop management practices.

This study provided a way to analyze the temporal characteristics between λET and affecting factors for varying underlying surfaces, which has increased our understanding of the water cycle at different time scales and provides a theoretical basis for the selection of estimation models at varying time scales to enhance water management.

Declaration of Competing Interest

The authors declare that they have no known competing financial interests or personal relationships that could have appeared to influence the work reported in this paper.

Data Availability

Data will be made available on request.

Acknowledgements

We acknowledge support from the National Natural Science Foundation of China (52179036, 52322904) and the Startup Foundation for Introducing Talent of Wuhan University (2042022rc0013). We sincerely appreciate Dr. Wei Hu for providing the code of partial wavelet coherence and suggestions.

References

- Allen, R.G., Pereira, L.S., Raes, D., Smith, M., 1998. Crop evapotranspiration-guidelines for computing crop water requirements. FAO Irrigation and Drainage. FAO, Rome, Italy.
- Baldocchi, D., Falge, E., Wilson, K., 2001. A spectral analysis of biosphere-atmosphere trace gas flux densities and meteorological variables across hour to multi-year time scales. *Agric. For. Meteorol.* 107 (1), 1–27. [https://doi.org/10.1016/S0168-1923\(00\)00228-8](https://doi.org/10.1016/S0168-1923(00)00228-8).
- Burba, G.G., Verma, S.B., 2005. Seasonal and interannual variability in evapotranspiration of native tallgrass prairie and cultivated wheat ecosystems. *Agric. For. Meteorol.* 135 (1), 190–201. <https://doi.org/10.1016/j.agrformet.2005.11.017>.

- Conway, G.R., 1987. The properties of agroecosystems. *Agric. Syst.* 24 (2), 95–117. [https://doi.org/10.1016/0308-521X\(87\)90056-4](https://doi.org/10.1016/0308-521X(87)90056-4).
- Ding, R., Kang, S., Vargas, R., Zhang, Y., Hao, X., 2013. Multiscale spectral analysis of temporal variability in evapotranspiration over irrigated cropland in an arid region. *Agric. Water Manag.* 130, 79–89. <https://doi.org/10.1016/j.agwat.2013.08.019>.
- Djaman, K., Balde, A.B., Sow, A., Muller, B., Irmak, S., N Diaye, M.K., Manneh, B., Moukoubi, Y.D., Futakuchi, K., Saito, K., 2015. Evaluation of sixteen reference evapotranspiration methods under sahelian conditions in the Senegal River Valley. *J. Hydrol. - Reg. Stud.* 3, 139–159. <https://doi.org/10.1016/j.ejrh.2015.02.002>.
- Fawen, L., Manjing, Z., Yong, Z., Rengui, J., 2023. Influence of irrigation and groundwater on the propagation of meteorological drought to agricultural drought. *Agric. Water Manag.* 277, 108099. <https://doi.org/10.1016/j.agwat.2022.108099>.
- Gill, L.W., Naughton, O., Johnston, P.M., Basu, B., Ghosh, B., 2013. Characterisation of hydrogeological connections in a lowland Karst network using time series analysis of water levels in ephemeral groundwater-fed lakes (turloughs). *J. Hydrol.* 499, 289–302. <https://doi.org/10.1016/j.jhydrol.2013.07.002>.
- Gong, X., Qiu, R., Zhang, B., Wang, S., Ge, J., Gao, S., Yang, Z., 2021. Energy budget for tomato plants grown in a greenhouse in northern China. *Agric. Water Manag.* 255, 107039. <https://doi.org/10.1016/j.agwat.2021.107039>.
- Grinsted, A., Moore, J.C., Jevrejeva, S., 2004. Application of the cross wavelet transform and wavelet coherence to geophysical time series. *Nonlinear Process. Geophys.* 11 (5/6), 561–566. <https://doi.org/10.5194/npg-11-561-2004>.
- Hickman, G.C., Vanloocke, A., Dohleman, F.G., Bernacchi, C.J., 2010. A comparison of canopy evapotranspiration for maize and two perennial grasses identified as potential bioenergy crops. *GCB Bioenergy* 2 (4), 157–168. <https://doi.org/10.1111/j.1757-1707.2010.01050.x>.
- Howell, T.A., Tolk, J.A., Schneider, A.D., Evett, S.R., 1998. Evapotranspiration, yield, and water use efficiency of corn hybrids differing in maturity. *Agron. J.* 90 (1), 3–9. <https://doi.org/10.2134/agonj1998.00021962009000010002x>.
- Hu, W., Si, B., 2021. Technical note: improved partial wavelet coherency for understanding scale-specific and localized bivariate relationships in geosciences. *Hydrol. Earth Syst. Sci.* 25 (1), 321–331. <https://doi.org/10.5194/hess-25-321-2021>.
- Hu, W., Si, B.C., 2016. Technical note: multiple wavelet coherence for untangling scale-specific and localized multivariate relationships in geosciences. *Hydrol. Earth Syst. Sci.* 20 (8), 3183–3191. <https://doi.org/10.5194/hess-20-3183-2016>.
- Hu, X., Lei, H., 2021. Evapotranspiration partitioning and its interannual variability over a winter wheat-summer maize rotation system in the North China Plain. *Agric. For. Meteorol.* 310, 108635. <https://doi.org/10.1016/j.agrformet.2021.108635>.
- Huang, L., Kemaq, Q., Pan, B., Asundi, A.K., 2010. Comparison of Fourier transform, windowed Fourier transform, and wavelet transform methods for phase extraction from a single fringe pattern in fringe projection profilometry. *Opt. Lasers Eng.* 48 (2), 141–148. <https://doi.org/10.1016/j.agrformet.2021.108635>.
- Kaimal, J.C., Wyngaard, J., Izumi, Y., Coté, O.R., 1972. Spectral characteristics of surface-layer turbulence. *J. R. Meteorol. Soc.* 98 (417), 563–589. <https://doi.org/10.1002/qj.49709841707>.
- Kang, S., Gu, B., Du, T., Zhang, J., 2003. Crop coefficient and ratio of transpiration to evapotranspiration of winter wheat and maize in a semi-humid region. *Agric. Water Manag.* 59 (3), 239–254. [https://doi.org/10.1016/S0378-3774\(02\)00150-6](https://doi.org/10.1016/S0378-3774(02)00150-6).
- Katul, G., Lai, C., Schäfer, K., Vidakovic, B., Albertson, J., Ellsworth, D., Oren, R., 2001. Multiscale analysis of vegetation surface fluxes: from seconds to years. *Adv. Water Resour.* 24 (9–10), 1119–1132. [https://doi.org/10.1016/S0309-1708\(01\)00029-X](https://doi.org/10.1016/S0309-1708(01)00029-X).
- Kiş, Ö., 2011. Evapotranspiration modeling using a wavelet regression model. *Irrig. Sci.* 29, 241–252. <https://doi.org/10.1007/s00271-010-0232-6>.
- Kumar, P., Foufoula Georgiou, E., 1997. Wavelet analysis for geophysical applications. *Rev. Geophys.* 35 (4), 385–412. <https://doi.org/10.1029/97RG00427>.
- Lei, H., Yang, D., 2010. Interannual and seasonal variability in evapotranspiration and energy partitioning over an irrigated cropland in the North China plain. *Agric. For. Meteorol.* 150 (4), 581–589. <https://doi.org/10.1016/j.agrformet.2010.01.022>.
- Li, M., Xia, J., Chen, Z., Meng, D., Xu, C., 2013. Variation analysis of precipitation during past 286 years in Beijing area, China, using non-parametric test and wavelet analysis. *Hydrol. Process.* 27 (20), 2934–2943. <https://doi.org/10.1002/hyp.9388>.
- Mallat, S., 1999. *A Wavelet Tour of Signal Processing*. Academic Press, pp. 1–637 (pp. I–XXIV).
- Mouatadid, S., Adamowski, J.F., Tiwari, M.K., Quilty, J.M., 2019. Coupling the maximum overlap discrete wavelet transform and long short-term memory networks for irrigation flow forecasting. *Agric. Water Manag.* 219, 72–85. <https://doi.org/10.1016/j.agwat.2019.03.045>.
- Partal, T., 2009. Modelling evapotranspiration using discrete wavelet transform and neural networks. *Hydrol. Process.* 23 (25), 3545–3555. <https://doi.org/10.1002/hyp.7448>.
- Perez, P.J., Castellvi, F., Ibanez, M., Rosell, J.I., 1999. Assessment of reliability of Bowen ratio method for partitioning fluxes. *Agric. For. Meteorol.* 97 (3), 141–150. [https://doi.org/10.1016/S0168-1923\(99\)00080-5](https://doi.org/10.1016/S0168-1923(99)00080-5).
- Qiu, R., Liu, C., Cui, N., Wu, Y., Wang, Z., Li, G., 2019. Evapotranspiration estimation using a modified Priestley-Taylor model in a rice-wheat rotation system. *Agric. Water Manag.* 224, 105755. <https://doi.org/10.1016/j.agwat.2019.105755>.
- Qiu, R., Katul, G., Wang, J., Xu, J., Kang, S., Liu, C., Zhang, B., Li, L., Cajucom, P., 2021. Differential response of rice evapotranspiration to varying patterns of warming. *Agric. For. Meteorol.* 298–299, 108293. <https://doi.org/10.1016/j.agrformet.2020.108293>.
- Qiu, R., Li, L., Liu, C., Wang, Z., Zhang, B., Liu, Z., 2022. Evapotranspiration estimation using a modified crop coefficient model in a rotated rice-winter wheat system. *Agric. Water Manag.* 264, 107501. <https://doi.org/10.1016/j.agwat.2022.107501>.
- Qiu, R., Luo, Y., Wu, J., Zhang, B., Liu, Z., Agathokleous, E., Yang, X., Hu, W., Clothier, B., 2023. Short-term forecasting of daily evapotranspiration from rice using a modified Priestley-Taylor model and public weather forecasts. *Agric. Water Manag.* 277, 108123. <https://doi.org/10.1016/j.agwat.2022.108123>.
- Rana, G., Katerji, N., 2000. Measurement and estimation of actual evapotranspiration in the field under Mediterranean climate: a review. *Eur. J. Agron.* 13 (2–3), 125–153. [https://doi.org/10.1016/S1161-0301\(00\)00070-8](https://doi.org/10.1016/S1161-0301(00)00070-8).
- Sen, A.K., 2009. Spectral-temporal characterization of riverflow variability in England and Wales for the period 1865–2002. *Hydrol. Process.* 23 (8), 1147–1157. <https://doi.org/10.1002/hyp.7224>.
- Sifuzzaman, M., Islam, M.R., Ali, M.Z., 2009. Application of wavelet transform and its advantages compared to Fourier transform. *J. Phys. Sci.* 13, 121–134.
- Steduto, P., Hsiao, T.C., 1998. Maize canopies under two soil water regimes: ii. Seasonal trends of evapotranspiration, carbon dioxide assimilation and canopy conductance, and as related to leaf area index. *Agric. For. Meteorol.* 89 (3–4), 185–200. [https://doi.org/10.1016/S0168-1923\(97\)00084-1](https://doi.org/10.1016/S0168-1923(97)00084-1).
- Sutanto, S.J., Weninger, J., Coenders-Gerrits, A., Uhlenbrook, S., 2012. Partitioning of evaporation into transpiration, soil evaporation and interception: a comparison between isotope measurements and a HYDRUS-1D model. *Hydrol. Earth Syst. Sci.* 16 (8), 2605–2616. <https://doi.org/10.5194/hess-16-2605-2012>.
- Suyker, A.E., Verma, S.B., 2008. Interannual water vapor and energy exchange in an irrigated maize-based agroecosystem. *Agric. For. Meteorol.* 148 (3), 417–427. <https://doi.org/10.1016/j.agrformet.2007.10.005>.
- Tang, Y., Jia, C., Wang, L., Wen, X., Wang, H., 2021. Solar energy dominates and soil water modulates net ecosystem productivity and evapotranspiration across multiple timescales in a subtropical coniferous plantation. *Agric. For. Meteorol.* 300, 108310. <https://doi.org/10.1016/j.agrformet.2020.108310>.
- Torrence, C., Compo, G.P., 1998. A practical guide to wavelet analysis. *Bull. Am. Meteorol. Soc.* 79 (1), 61–78. [https://doi.org/10.1175/1520-0477\(1998\)079<0061:APGTWA>2.0.CO;2](https://doi.org/10.1175/1520-0477(1998)079<0061:APGTWA>2.0.CO;2).
- Tyagi, N.K., Sharma, D.K., Luthra, S.K., 2000. Determination of evapotranspiration and crop coefficients of rice and sunflower with lysimeter. *Agric. Water Manag.* 45 (1), 41–54. [https://doi.org/10.1016/S0378-3774\(99\)00071-2](https://doi.org/10.1016/S0378-3774(99)00071-2).
- Vargas, R., Detto, M., Baldocchi, D.D., Allen, M.F., 2010. Multiscale analysis of temporal variability of soil CO₂ production as influenced by weather and vegetation. *Glob. Change Biol.* 16 (5), 1589–1605. <https://doi.org/10.1111/j.1365-2486.2009.02111.x>.
- Wang, F., Lai, H., Li, Y., Feng, K., Zhang, Z., Tian, Q., Zhu, X., Yang, H., 2022. Dynamic variation of meteorological drought and its relationships with agricultural drought across China. *Agric. Water Manag.* 261, 107301. <https://doi.org/10.1016/j.agwat.2021.107301>.
- Yan, H., Li, M., Zhang, C., Zhang, J., Wang, G., Yu, J., Ma, J., Zhao, S., 2022. Comparison of evapotranspiration upscaling methods from instantaneous to daytime scale for tea and wheat in southeast China. *Agric. Water Manag.* 264, 107464. <https://doi.org/10.1016/j.agwat.2022.107464>.
- Yang, F., Zhang, Q., Wang, R., Zhou, J., 2014. Evapotranspiration measurement and crop coefficient estimation over a spring wheat farmland ecosystem in the Loess Plateau. *PLoS One* 9 (6), e100031. <https://doi.org/10.1371/journal.pone.0100031>.
- Yoshida, M., Ohta, T., Kotani, A., Maximov, T., 2010. Environmental factors controlling forest evapotranspiration and surface conductance on a multi-temporal scale in growing seasons of a Siberian larch forest. *J. Hydrol.* 395 (3–4), 180–189. <https://doi.org/10.1016/j.jhydrol.2010.10.023>.
- Zhang, X., Chen, S., Sun, H., Shao, L., Wang, Y., 2011. Changes in evapotranspiration over irrigated winter wheat and maize in North China Plain over three decades. *Agric. Water Manag.* 98 (6), 1097–1104. <https://doi.org/10.1016/j.agwat.2011.02.003>.
- Zhou, Z., Liu, S., Ding, Y., Fu, Q., Wang, Y., Cai, H., Shi, H., 2022. Assessing the responses of vegetation to meteorological drought and its influencing factors with partial wavelet coherence analysis. *J. Environ. Manag.* 311, 114879. <https://doi.org/10.1016/j.jenvman.2022.114879>.